




RESEARCH ARTICLE | FEBRUARY 16 2021

# Curry–Yorke route to shearless attractors and coexistence of attractors in dissipative nontwist systems

Special Collection: [Recent Advances in Modeling Complex Systems: Theory and Applications](#)

Michele Mugnaine ; Antonio M. Batista; Iberê L. Caldas ; José D. Szezech, Jr.  ; Ricardo Egdio de Carvalho; Ricardo L. Viana 



Chaos 31, 023125 (2021)

<https://doi.org/10.1063/5.0035303>



View  
Online



Export  
Citation

CrossMark



**Chaos**  
Special Topic: Advances in  
Adaptive Dynamical Networks  
**Submit Today**



# Curry–Yorke route to shearless attractors and coexistence of attractors in dissipative nontwist systems

Cite as: Chaos 31, 023125 (2021); doi: 10.1063/5.0035303

Submitted: 27 October 2020 · Accepted: 22 January 2021 ·

Published Online: 16 February 2021







View Online



Export Citation



CrossMark

Michele Mugnaine,<sup>1</sup>  Antonio M. Batista,<sup>2,3,4</sup> Iberê L. Caldas,<sup>4</sup>  José D. Szezech, Jr.,<sup>2,3,a)</sup>   
Ricardo Egydio de Carvalho,<sup>5</sup> and Ricardo L. Viana<sup>1</sup> 

## AFFILIATIONS

<sup>1</sup>Department of Physics, Federal University of Paraná, 80060-000 Curitiba, PR, Brazil

<sup>2</sup>Department of Mathematics and Statistics, State University of Ponta Grossa, 84030-900 Ponta Grossa, PR, Brazil

<sup>3</sup>Graduate in Science Program—Physics, State University of Ponta Grossa, 84030-900 Ponta Grossa, PR, Brazil

<sup>4</sup>Institute of Physics, University of São Paulo, 05508-900 São Paulo, SP, Brazil

<sup>5</sup>Department of Statistics, Applied Mathematics and Computer Science, Institute of Geosciences and Exact Sciences—IGCE, São Paulo State University (UNESP), 13506-900 Rio Claro, SP, Brazil

**Note:** This paper is part of the Focus Issue, Recent Advances in Modeling Complex Systems: Theory and Applications.

**a) Author to whom correspondence should be addressed:** [jdsjunior@uepg.br](mailto:jdsjunior@uepg.br)

## ABSTRACT

The routes to chaos play an important role in predictions about the transitions from regular to irregular behavior in nonlinear dynamical systems, such as electrical oscillators, chemical reactions, biomedical rhythms, and nonlinear wave coupling. Of special interest are dissipative systems obtained by adding a dissipation term in a given Hamiltonian system. If the latter satisfies the so-called twist property, the corresponding dissipative version can be called a “dissipative twist system.” Transitions to chaos in these systems are well established; for instance, the Curry–Yorke route describes the transition from a quasiperiodic attractor on torus to chaos passing by a chaotic banded attractor. In this paper, we study the transitions from an attractor on torus to chaotic motion in dissipative nontwist systems. We choose the dissipative standard nontwist map, which is a non-conservative version of the standard nontwist map. In our simulations, we observe the same transition to chaos that happens in twist systems, known as a soft one, where the quasiperiodic attractor becomes wrinkled and then chaotic through the Curry–Yorke route. By the Lyapunov exponent, we study the nature of the orbits for a different set of parameters, and we observe that quasiperiodic motion and periodic and chaotic behavior are possible in the system. We observe that they can coexist in the phase space, implying in multistability. The different coexistence scenarios were studied by the basin entropy and by the boundary basin entropy.

Published under license by AIP Publishing. <https://doi.org/10.1063/5.0035303>

Conservative systems belong to a class of dynamical systems that have been studied in classical mechanics and electrodynamics. One simple and general example of conservative system is the nontwist map. It does not satisfy the twist condition and has been used to describe various physical phenomena related to particle accelerators and plasma devices. The nontwist map exhibits meandering invariant tori, separatrix reconnection, and shearless tori. It was reported that dissipation in the nontwist map turns the shearless curve into a robust attractor, called as a shearless attractor. Given the ubiquitous nature of dissipation, however, it is of interest in the study of conservative systems in which a small dissipative term has been added. In this case, we can call the resulting system as a “dissipative nontwist” one. Here, we

study the dynamical behavior of the dissipative standard nontwist map. We find the Curry–Yorke route to shearless attractors, which occurs due to the destabilization of a two-dimensional torus. This route was observed in laser with delayed feedback and a driven double scroll circuit. Through the Lyapunov exponent, we identify the coexistence of attractor basins and their different interaction scenarios using the basin entropy.

## I. INTRODUCTION

Conservative dynamical systems belong to a wide class of systems that describe physical phenomena in which the dissipation

can be neglected. Inside this class, the Hamiltonian description is a valuable tool to study the solutions and the time evolution of the system. The behavior of fields and particles and classical and quantum objects can be analyzed and studied by integrable Hamiltonian systems.<sup>1</sup> However, when a perturbation breaks the Hamiltonian integrability, the chaotic motion becomes a possible solution for the system, along with the periodic and quasiperiodic solutions. The perturbed conservative systems require a more sophisticated mathematics to study the evolution of the regular orbits. The beginning of this new mathematical development started with Poincaré with his work on the existence of invariant surfaces, the tori, and their destruction as a consequence of perturbation.<sup>2–4</sup> The work started by Poincaré was concluded by Birkhoff<sup>3</sup> in the famous Poincaré–Birkhoff theorem, which was established in the first half of the 20th century.

Following the second half of the last century, Kolmogorov, Arnold, and Moser achieved one of the most celebrated progress in classical mechanics, the KAM theorem.<sup>2–4</sup> The KAM theorem provides a solid foundation to the study of regular motion in Hamiltonian systems<sup>5</sup> and also gives meaning to perturbation theory and the notion of chaos.<sup>4</sup> Along with the Poincaré–Birkhoff theorem, these theorems describe the dynamics of quasiperiodic and periodic solutions under the action of external perturbations. Both theorems are general and valid for many dynamical systems but not for all of them. One of the necessary and essential conditions for the KAM and Poincaré–Birkhoff theorems to be valid is the twist condition, which needs to be globally satisfied. The twist condition is applied in Hamiltonian dynamics described by map and differential equation models.<sup>4</sup> Considering the latter, the Hamiltonian of a perturbed Hamiltonian system with one and a half degrees of freedom can be written as

$$H = H_0(J) + \varepsilon H_1(\theta, J, t), \quad (1)$$

where  $(J, \theta)$  are the action-angle variables and  $\varepsilon \ll 1$ .<sup>4</sup> Once the frequency can be defined as  $\omega(J) = \partial H_0 / \partial J$ , the twist condition is stated as

$$\left| \frac{\partial \omega(J)}{\partial J} \right| > 0, \quad (2)$$

ensuring that the frequency has a monotonic behavior. For a discrete description of the Hamiltonian system, the twist condition can be defined as  $|\partial y_{n+1} / \partial x_n| > 0$ , where  $x$  and  $y$  are the canonically conjugate coordinates of the map.

If at one point in the phase space the twist condition (2) is violated, i.e., it is equal to zero, the frequency  $\omega(J)$  is no longer monotonic. It exhibits an extreme value and the system is denominated nontwist.<sup>4</sup> Nontwist systems are useful to describe several physical phenomena, such as magnetic field lines in toroidal plasma devices, atmospheric zonal flows, and others.<sup>4,6</sup> The violation of the twist condition occurs over a specific curve in the phase space, the shearless curve, and it leads to the existence of a new and rich behavior in the space, as the presence of twin island chains (the down and up periodic orbits), the separatrix and stochasticity layer reconnection, and the collision of periodic orbits.<sup>6,7</sup>

The universal features of the nontwist systems can be represented by the characteristics of the standard nontwist map (SNM), which was proposed by Castillo-Negrete and Morrison in their study

published in 1993.<sup>7</sup> The SNM is a two-dimensional conservative perturbed system that violates the twist condition and exhibits a two-parameter dependence. The properties of the SNM were widely studied in the last few decades, such as the reconnection and the bifurcation phenomena of meanders,<sup>6</sup> the symmetry properties, the collision of periodic orbits and the transition to chaos,<sup>8</sup> the transport properties and the transport mechanism,<sup>9–12</sup> and also expansions and modifications in the SNM.<sup>13–17</sup>

The dissipation in nontwist Hamiltonian systems is of practical interest once real experiments often present a small amount of dissipation.<sup>18</sup> The introduction of dissipation in nontwist systems was considered by Van der Weele and Valkering in a work published in 1990.<sup>18</sup> The authors studied the influence of the dissipation in the birth of periodic orbits and in the reconnection process in nontwist maps. The dissipation was also included by Carvalho and Abud in the labyrinthical standard nontwist map (LSNM),<sup>14</sup> first described without dissipation in Refs. 13 and 19, with the purpose of understanding the dynamics of the shearless curve in a non-conservative scenario. As stated in Refs. 14 and 15, the shearless curve becomes a shearless attractor on a torus and can show a chaotic behavior for some set of parameters.

For twist systems, the transition from a quasiperiodic to chaotic attractor on a torus is well established. In general, this transition occurs when the torus breaks up and it can happen in many different ways. Letellier *et al.* analyzed the transition to chaos on a periodically driven van der Pol oscillator that can be interpreted, in a simplified way, by the Curry–Yorke map.<sup>20</sup> In this study, they established two routes from quasiperiodic motion to a chaotic behavior on a torus. The first route is the “hard” transition to chaos, which involves the wrinkling of the torus and then its replacement by a chaotic attractor. The second route is the “soft” one, where after the wrinkling, a banded chaotic attractor structure is settled and then the chaotic attractor emerges.<sup>20,21</sup> We will use this designation of “soft” and “hard” transitions defined by Letellier in Ref. 20 in our study. The soft transition is also nominated as the “Curry–Yorke route,” first discussed by Curry and Yorke in 1978.<sup>22</sup> The route was also investigated in a global bifurcation scenario<sup>23,24</sup> and applied in examples as van der Pol oscillators<sup>20</sup> and the driver double scroll circuit.<sup>21</sup>

In this survey, we choose the dissipative standard nontwist system, namely, the SNM with a controllable dissipation, to study the evolution of attractors when parameters of the system are changed. We find the Curry–Yorke route to chaos, in which the attractor is wrinkled, as a parameter is varied, and the chaotic behavior of the attractor on the torus appears. We also show the coexistence of attractors in the phase space, and we analyze the coexistence scenario by the basin entropy and the boundary basin entropy.

The paper is organized as follows. In Sec. II, we describe our chosen system and analyze the diagram bifurcation in such a way that it is possible to find a hard transition to chaos. The Curry–Yorke route is explained in Sec. III, and we show this scenario through the dissipative standard nontwist map. Section IV is dedicated to the study of the nature of the attractors in the phase space by the analysis of the Lyapunov exponent and the period counting. We also study the possibility of multiple attractors and their basins of attraction. The results of multistability are shown in Sec. V. Our conclusions are left to Sec. VI.

## II. DISSIPATIVE STANDARD NONTWIST MAP

The labyrinthic standard nontwist map (LSNM) was proposed<sup>13,19</sup> as a novel discrete area-preserving map that can be used to study the features of nontwist systems. The map was studied first in Refs. 13 and 19. It was considered in a dissipative scenario by Carvalho and Abud<sup>14</sup> and was revisited in Ref. 15. The LSNM, presented in Refs. 14 and 15, is defined by the equations

$$\begin{aligned} y_{n+1} &= (1 - \gamma)y_n - b[\sin(2\pi x_n) + \sin(2\eta\pi x_n)], \\ x_{n+1} &= x_n - a(y_{n+1} - r_1)(y_{n+1} - r_2). \end{aligned} \tag{3}$$

In Eq. (3), the parameters  $\gamma$ ,  $a$ , and  $b$  are responsible for the dissipation, for the influence control of the nontwist term, and for the amplitude control of the non-linearity, respectively.<sup>15</sup> The parameters  $a$  and  $b$  affect the amplitude of the islands and the size of the chaotic sea.<sup>14</sup> The parameters  $r_1$  and  $r_2$  indicate the location where the resonances will appear in the phase space.<sup>15</sup> Finally,  $\eta$  is responsible for the bifurcations inside the resonance islands.<sup>15</sup> The variable  $x$  has a period equal to 1,  $x \in [0, 1)$ , and the twist condition is violated when  $\frac{\partial x_{n+1}}{\partial y_n} \neq 0$  is satisfied.

According to Martins *et al.*,<sup>13</sup> the LSNM exhibits all properties of the usual nontwist maps and the possibility of several regions with meanders. Meanders correspond to the invariant curves that are no longer graphs in the phase space once they exhibit two values of  $y$  for one value of  $x$ .<sup>19</sup> For the conservative LSNM, the Hamiltonian function is given by<sup>13</sup>

$$\begin{aligned} H(x, y, t) &= \left[ a \left( y - \frac{y^3}{3} \right) \right] + \frac{b}{2\pi} \cos(2\pi x) \sum_{n=-\infty}^{\infty} \delta(t - n) \\ &+ \frac{b}{\eta 2\pi} \cos(2\eta\pi x) \sum_{n=-\infty}^{\infty} \delta(t - n). \end{aligned} \tag{4}$$

The function in (4) is constituted by the Hamiltonian of the standard nontwist map (SNM) with the addition of a perturbation (last term)<sup>7</sup>. The amplitude control of the non-linearity is described by a rotor kicked periodically by a Dirac delta function, where the discrete iterative map in Eq. (3) is obtained from these successive periodic kicks. The SNM is the simplest nontwist map that exhibits the main nontwist characteristics and is considered an approximation for more complex nontwist systems.<sup>25</sup>

As concluded by Martins *et al.*, the perturbation introduced as the last term in (4) interacts with the first perturbation represented by the second term. Due to this fact, new topological effects emerge; i.e., plenty meanders regions coexist, where each region presents its own shearless torus.<sup>13</sup>

Once our goal is to understand the effects of the presence of the dissipation and the route to chaos in nontwist systems, we simplify the LSNM in (3) by setting  $\eta = 0$ ,  $r_1 = 1$ , and  $r_2 = -1$ . In this way, we obtain

$$\begin{aligned} y_{n+1} &= (1 - \gamma)y_n - b \sin(2\pi x_n), \\ x_{n+1} &= x_n + a(1 - y_{n+1}^2) \pmod{1}. \end{aligned} \tag{5}$$

For  $\gamma = 0$ , we recover the nontwist standard map (SNM). In this way, for  $\gamma \neq 0$ , we have dissipation in the SNM and, consequently,

the dissipative standard nontwist map (DSNM). As the SNM is considered the simplest conservative nontwist system and an approximation to more complex models, we can say that the DSNM is the simplest dissipative nontwist map, and the results obtained for it can be extended to more complex dissipative cases. Therefore, we chose the DSNM to study the consequences of dissipation in a nontwist system and the loss of the constant of motion represented by the Hamiltonian function so that the DSNM is no longer invertible in time such as autonomous Hamiltonian systems.

As demonstrated by Carvalho and Abud,<sup>14</sup> in the perturbed dissipative LSNM, the shearless curve survives a perturbation, as long as it is not very large, and becomes an attractor in the phase space. The shearless curve is the representation of the quasiperiodic shearless torus in the Poincaré section. Therefore, the shearless attractor is an attractor on a torus. For different values of the parameters, the quasiperiodic behavior on a torus can transit to a chaotic behavior, leading to a chaotic attractor (or a strange attractor).

Another interesting feature in the LSNM presented by Kato and De Carvalho,<sup>15</sup> it is the possibility of multiple shearless attractors forming, in this way, a region of robust attractors. The shearless attractors are considered robust due to their origin on shearless torus and due to the fact that they survive under generic perturbations and different intensities of the dissipation.<sup>14,15</sup> In order to illustrate the shearless attractor and the consequence of dissipation in the standard nontwist map, we construct the phase space for the conservative ( $\gamma = 0.0$ ) and the dissipative cases ( $\gamma = 0.1$ ) with parameters  $a = 0.47$  and  $b = 0.6$ . The two phase spaces are shown in Fig. 1.

In Fig. 1(a), once the Hamiltonian system is perturbed, a coexistence of chaotic (black points), quasi-regular (blue and red curves), and regular (colored islands) solutions is present in the phase space. The red curve in Fig. 1(a) is the shearless curve: the curve where the twist condition is violated and is constructed by the indicator point  $z = (-\frac{1}{4}, -\frac{b}{2})$  as the initial condition.<sup>6,26</sup> When the dissipation is considered, the conservative phase space in Fig. 1(a) becomes the attractors in Fig. 1(b). Comparing the two figures, we can see that the upper (lower) periodic solution, indicated by the purple (orange) islands, becomes fixed point attractors, the purple (orange) point, while almost all of the quasiperiodic solutions are destroyed and replaced by only one attractor: the shearless attractor, represented by the black curve in Fig. 1(b).

The attractors of the dissipative LSNM were reported in the papers.<sup>14,15</sup> In Ref. 14, the authors showed the presence of a shearless attractor resultant of the dissipation of a shearless curve. However, another interesting point is the presence of different behaviors in this attractor on the torus, in which the attractor can change from quasiperiodic to chaotic.<sup>14</sup> In this paper, we develop a similar study for the DSNM [Eq. (5)]. Once we consider dissipation in the standard nontwist map, it has attractors in the phase space. We compute the bifurcation diagram, for a fixed value of  $b$ , in order to investigate the shapes and structures of the attractors along the variation of the parameter  $a$ . In the diagram, as shown in Fig. 2, we fix a set of parameters ( $a, b$ ) and one initial condition is iterated for a long time. We plot the values of  $y$  for the last iterations and different values of  $a$ . The initial condition is chosen according to the methodology used by Letellier *et al.*<sup>20</sup> For each change in the parameter  $a$ , the initial condition  $(x_0, y_0)$  for the next parameter value is the same as the last iteration of the previous one. For the bifurcation

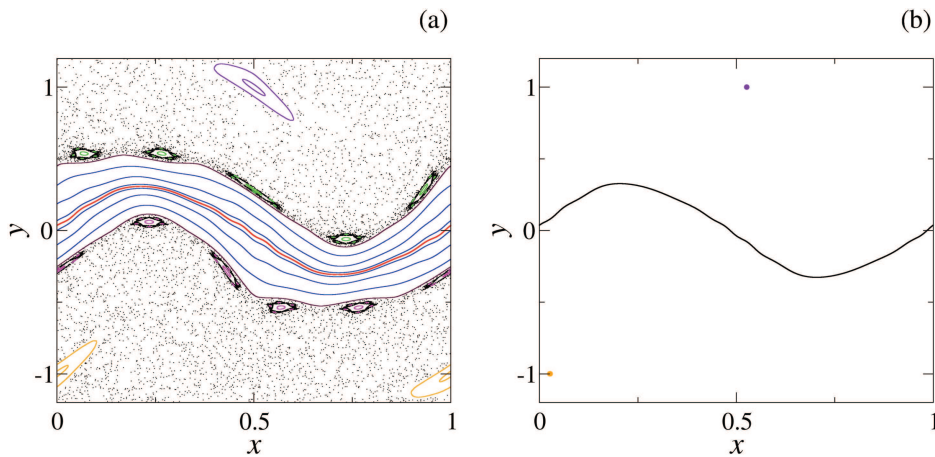


**FIG. 1.** Phase spaces for the (a) conservative map and the (b) dissipative system. The parameters are  $a = 0.47$  and  $b = 0.6$  for both cases, and we considered  $\gamma = 0.1$  for the dissipative scenario. The coexistence of chaotic (disperse points), quasiperiodic (blue and red curves), and periodic (colored closed curves) solutions in the phase space is observed for the conservative case. When the dissipation is present, we observe only a quasiperiodic attractor and two period-one fixed points (orange and purple points). The shearless curve (attractor) is indicated by the red (black) curve in (a) [(b)].

diagrams, we take as the first initial condition, for the first value of  $a$ , the indicator point of the non-dissipative standard nontwist map  $z = (-\frac{1}{4}, -\frac{b}{2})$ .<sup>6,26</sup> As the final iteration, we consider  $n = 10^4$  and plot the last 2000 iterations in the diagram.

Along with the bifurcation diagram, we plot the Lyapunov exponent value for the orbit in the diagram. The Lyapunov exponent provides us an estimate of the exponential separation between trajectories with close initial conditions.<sup>27</sup> For a discrete time dynamical system, the map is defined by  $f(x)$ , and the matrix of partial derivatives of the  $m$  components of  $f(x)$  is denoted by  $T(x)$ .<sup>27</sup> The largest Lyapunov exponent is determined by the limit

$$\lambda_1 = \lim_{n \rightarrow \infty} \frac{1}{n} \log \|T_x^n u\|, \tag{6}$$

where  $T_x^n = T(f^{n-1}(x))T(f^{n-2}(x)) \cdots T(f(x))T(x)$  is the product of the matrix of derivatives for each time step and  $u$  is an eigenvector of  $T_x^n$ .<sup>9,27</sup> More details of how the calculation is done computationally can be found in Refs. 27–29. A null Lyapunov exponent indicates quasiperiodic attractors, while a negative exponent implies a periodic attractor, and a positive one indicates chaos or a chaotic attractor. The Lyapunov exponent is computed simultaneously with the bifurcation diagram. The Lyapunov exponents are calculated according to the method proposed by Eckmann and Ruelle,<sup>27</sup> disregarding the first 5000 iterations until the final time  $n = 10^4$ . The results of the bifurcation diagram and the Lyapunov exponent are shown in Fig. 2 for  $b = 0.58$  and  $a \in [0.7, 0.715]$ .

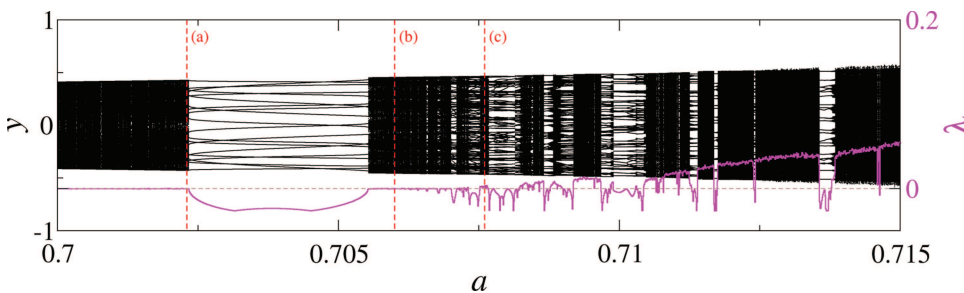


**FIG. 2.** Bifurcation diagram for  $b = 0.58$  and  $\gamma = 0.1$ , where the black points indicate the last 2000 iterations of the orbit. The pink curve represents the Lyapunov exponent computed simultaneously for the orbit plotted in the diagram. The axis for the diagram (Lyapunov exponent) is in the left (right). The red vertical dashed lines correspond to the values of parameters: (a)  $a = 0.7023$ , (b)  $a = 0.7060$ , and (c)  $a = 0.7076$ .

The bifurcation diagram in Fig. 2 exhibits a set of different behaviors. Close to  $a = 0.7$ , we observe attractors that occupy and fill a range in the  $y$  domain until the point indicated by the red dashed line (a). After this point, we see distinguishable points, and then the attractor is only in some points in  $y$ . These two structures alternate along the entire diagram. For the first structure, it can represent two possible situations: a shearless attractor<sup>14</sup> or a chaotic behavior (a chaotic attractor or a chaotic solution with  $y$  restricted). Differently from the last case, the second structure indicates periodic attractors in the phase space, namely, distinct points where the solution is attracted and then jumps to one and then to another point repeatedly until completes its period. Analyzing the Lyapunov exponent, for the periodic attractors, their values are always negative. The null Lyapunov exponent happens when the attractors fill a  $y$ -range, suggesting a quasiperiodic orbit, or a bifurcation happens. The regions of a positive Lyapunov exponent often occur on the right side of the graph, indicating some kind of chaotic behavior. To identify and discern these behaviors, especially in the first case when the Lyapunov exponent is equal to zero, we check carefully the solutions in the phase space. To illustrate the different scenarios, we choose three parameter values in the bifurcation diagram, which are indicated by the red dashed lines (a)–(c), and we construct the phase spaces. The three phase spaces are shown in Fig. 3.

The phase spaces in Fig. 3 follow one of the routes cited by Letellier *et al.*,<sup>20</sup> the route with a hard transition to chaos. In Fig. 3(a), the attractor is a curve, namely, a meander in the phase space, and, as Carvalho and Abud named,<sup>14</sup> it is the shearless attractor



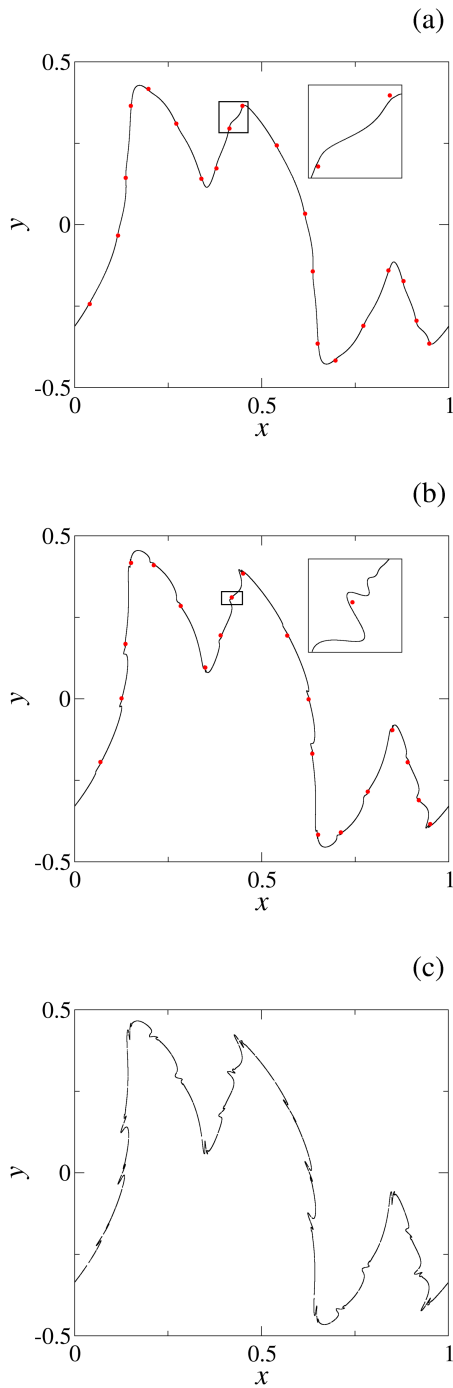


**FIG. 3.** Attractors and ghosts for the cases marked in Fig. 2. The cases are (a)  $a = 0.7023$  (ghost  $a = 0.7030$ ), (b)  $a = 0.7060$  (ghost  $a = 0.7050$ ), and (c)  $a = 0.7076$ . For all cases, the attractor on the torus is represented by the black curves and the ghost attractors are pictured by the red points, and we consider  $b = 0.58$  and  $\gamma = 0.1$ .

once its shape is similar to the shearless curve in the conservative case. Therefore, when the attractor fills a  $y$ -range and the respective Lyapunov exponent is null, we have the shearless attractor. The red points are denominated “ghosts” and represent stable orbits for nearby parameter values.<sup>20</sup> These ghosts are fixed points responsible for a large invariant density on the attractor, which is significant for the dynamics in the phase space.<sup>20</sup> In Fig. 3(a), there are periodic attractors for a posterior value of the parameter  $a$  for which the shearless attractor no longer exists. For the second phase space, in Fig. 3(b), we verify that the shearless attractor is wrinkled, and, if we analyze the magnification (the box in the upper right corner), the wrinkles are close to the ghost periodic points. In this case [Fig. 3(b)], the ghost points are periodic points for a previous parameter  $a$ . For both cases, the ghost points are one chain of fixed points with period 20. In the last phase space, Fig. 3(c), the attractor shows a shape similar to the attractor in Fig. 3(a). However, if we check the value of the Lyapunov exponent in Fig. 2 for the (c) red dashed line, we see that the value is small but is greater than zero. In this way, the attractor is chaotic in (c). If we pay attention to the Lyapunov exponent for the other two points, the exponents are null, and this is correct once there is a shearless attractor in (a) and (b). Summarizing, as the parameter value  $a$  increases, the attractor that was smooth becomes wrinkled and then chaotic. Observing the phase space in (a) and (b), we can see that the presence of the ghost points affects the shape of the attractor, as also verified by Letellier *et al.*<sup>20</sup>

### III. CURRY-YORKE ROUTE

In the study developed by Letellier *et al.*,<sup>20</sup> a “hard” route to the chaos and a “soft” route were identified in which the chaotic behavior on the torus emerges after the wrinkling. In Sec. II, we found the hard transition to chaos. Now, we search for the presence of the other route. The second route, also called the Curry–Yorke route, is a transition from quasiperiodic behavior to chaotic motion by the breakup of the torus, leading to a banded chaotic attractor and then to the chaotic attractor on a torus.<sup>20</sup> In order to look for the soft transition, we slightly modify the value of  $b$  to  $b = 0.6$ . Following the same steps, we build the bifurcation diagram and superimpose the Lyapunov exponent on it. We follow the same methodology used in Fig. 2, as shown in Fig. 4 for  $b = 0.6$ .

The bifurcation diagram in Fig. 4 also shows a set of different behaviors. Similarly to Fig. 2, we see the two structures already seen. The attractors occupy and fill the  $y$ -range and the periodic attractors, which are represented by distinguishable points, alternate along the diagram, as the value of  $a$  increases. However, for the last values of  $a$  in the diagram, we observe a slightly different behavior, namely, dispersed points in the  $y$  direction. Equally to Fig. 2, for small values of  $a$ , the attractors that fill the  $y$ -direction have a null Lyapunov exponent, indicating the quasiperiodic shearless attractors. The distinguishable points are periodic attractors with a negative Lyapunov exponent, and for greater values of  $a$ , we verify the existence of attractors and chaotic windows ( $a > 0.713$ ) with a positive Lyapunov exponent. In order to investigate the shape of those attractors, we choose three points ( $a, b = 0.6$ ), which are indicated by the three red dashed lines, and construct the phase spaces for each case, as shown in Fig. 5.

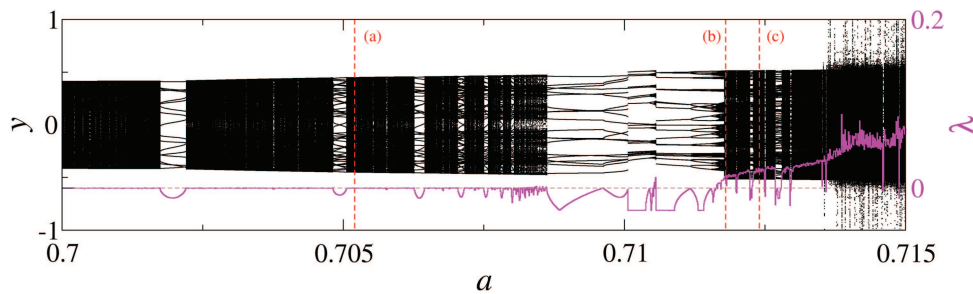


**FIG. 4.** Bifurcation diagram and the Lyapunov exponent vs the parameter  $a$  for  $b = 0.6$  and  $\gamma = 0.1$ . The quasiperiodic and periodic attractor alternates between each other until a chaotic behavior appears in the right side of the diagram. As in Fig. 2, the black and pink points indicate the diagram and the Lyapunov exponent. The red vertical dashed lines correspond to the values of parameters: (a)  $a = 0.7052$ , (b)  $a = 0.7118$ , and (c)  $a = 0.7124$ .

Analyzing the structures in each phase space in Fig. 5, we see in (a) an attractor in a meander, which is a smooth quasiperiodic shearless attractor surrounded by ghost fixed points. Again, these ghosts are periodic attractors of a posterior parameter, in this case  $a = 0.7063$ . These ghost points are the red and blue points, and both have period 37. In this case, we have two chains of fixed points (the red and the blue one), which is a dissipative correspondent for the twin island chains of the conservative map. Slightly increasing the value of  $a$  and comparing with the result in Fig. 3(b), we observe a different scenario. In Fig. 5(b), we verify many separated structures in the phase space closed to the ghost periodic attractors of a previous parameter. Here, the period of the ghost points is 40, and, as we can verify in the magnification in Fig. 5(b), it seems that they suffer a double-period bifurcation once there are two fixed points really closed. It is important to emphasize that a single orbit visits all the black separated structures, called bands, leading to a phase-locking scenario. Going back to the Lyapunov exponent for the case (b) in Fig. 4, we see that its value is positive for the banded attractor. In the last phase space, Fig. 5(c), we observe an attractor with a more complex shape and, by the Lyapunov exponent in Fig. 4, the attractor is chaotic. In this sequence of the phase space, we see the Curry–Yorke route<sup>23</sup> or the “soft” transition to chaos<sup>20</sup> in which the attractor on a “torus” is destabilized and followed by a sequence of phase-locking (banded attractor) and then chaos emerges.<sup>23</sup>

The existence of the same transition to chaos in both twist and nontwist systems is an interesting result. The quasiperiodic attractor acts similarly to the shearless curve, while the periodic ghost attractors can be divided into two twin chains of periodic points, which is an inherent feature of nontwist systems.<sup>30</sup> The main point of the two last sections is that the “hard” transition to chaos, smooth attractor  $\rightarrow$  wrinkled attractor  $\rightarrow$  chaotic attractor, and the “soft” transition (or Curry–Yorke route), smooth attractor  $\rightarrow$  chaotic banded attractor,  $\rightarrow$  chaotic attractor, are both possible to be found in systems that violate the twist condition.

#### IV. ORBIT ANALYSIS AND THE PARAMETER SPACE

The analysis of the phase space performed in the last section, by means of the Lyapunov exponent and the bifurcation diagram perspective, was restricted to a fixed value for  $b$  and a short range of  $a$ . Fixing  $\gamma = 0.1$  in our simulations, the DSNM depends on  $a$  and

$b$ . The study of bifurcation routes in the systems depending on two parameters can reveal nontrivial paths in the parameter space.<sup>20</sup> Our purpose in this section is to study the nature of the solutions in the phase space for each parameter pair  $(a, b)$ .

Bifurcation diagrams are commonly used to study the bifurcation route when only one parameter varies. The study of these diagrams when two parameters are varied is possible; however, it is not simple or easy to visualize and analyze. For this reason, we choose to study only the Lyapunov exponent. Thus, we calculate the Lyapunov exponent for each pair  $(a, b)$  with  $a \in [0, 1]$  and  $b \in [0, 1]$ , and its value is marked through a color scale in the parameter space  $a \times b$ .

To construct the parameter space, first, we fix a value for the parameter  $a$  and then we choose the indicator point of the conservative standard nontwist map  $z = (-\frac{1}{4}, -\frac{b}{2})$ , as an initial guess, for the first value of  $b$ . We iterate this condition until the final iteration  $n = 10^4$ , neglecting the first 5000 iterations, and calculate the Lyapunov exponent  $\lambda$  by the Eckmann and Ruelle method<sup>27</sup> for the last 5000 iterations. The final value of the Lyapunov exponent is plotted in the parameter space according to a color scale. For the next value of  $b$ , the last iteration  $(x, y)$  of the previous parameter is used as an initial condition, and the computation of  $\lambda$  is repeated until  $b = 1.0$ . For the next value of  $a$ , we restart the initial condition for the indicator point  $z$ , and all the process is repeated. In the parameter spaces shown in Fig. 6, we use a linear grid of  $2000 \times 2000$  points  $(a, b)$ .

In Fig. 6(a), we see the overview for  $a, b \in [0, 1]$ . The black dots represent the solution with a null Lyapunov exponent (quasiperiodic attractors). In general, the black dotted structure indicates the existence of a shearless attractor and is really similar to the parameter space for the existence of the shearless curve for the non-dissipative standard nontwist map.<sup>6</sup> The comparison between the parameter space for the shearless curve and the shearless attractor fails for small values of  $a$  where, for the conservative case, the shearless curve is present and for the dissipative case, there is a tendency for the orbits to be attracted to periodic attractors. We use the word “tendency” because we still cannot prove rigorously that there exists only one attractor in the phase space.

For larger values of  $a$  in the parameter space, we verify a significant tendency for a chaotic behavior in the phase space. We choose red, orange, and purple dots to represent the positive Lyapunov

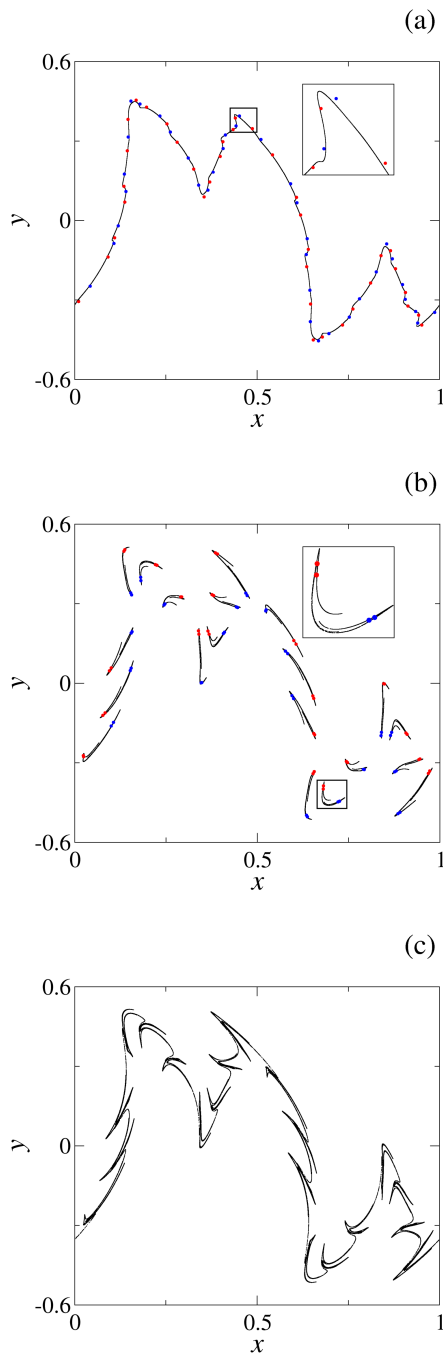


**FIG. 5.** The route to chaos for  $b = 0.6$ . For (a)  $a = 0.7052$ , the smooth quasiperiodic attractor on the torus is represented by the black curve, and there are two chains of a ghost periodic attractor, indicated by the blue and red points. In (b), we have  $a = 0.7118$ ; there are chaotic banded attractors, and the ghost attractors are two chains of period-40. For (c)  $a = 0.7124$ , there is only one chaotic attractor on the torus. The ghosts in (a) and (b) are shown for  $a = 0.7063$  and  $a = 0.7112$ , respectively.

exponent. The red dots indicate exponent values between  $0 < \lambda < 0.03$ , while the orange region represents  $0.03 < \lambda < 0.18$ , and the purple region is for  $\lambda > 0.18$ . The banded chaotic attractor [Fig. 5(b)] solution has a relatively small positive Lyapunov exponent,  $\lambda \approx 0.02$ . In this way, the red dots indicate possible points for chaotic band existence.

The magnification in Fig. 6(b) highlights the region of the bifurcation diagrams in Figs. 2 and 4. The white lines represent the lines along which those bifurcation diagrams are calculated. We see in both lines that there is a transition from the quasiperiodic attractor to a periodic one. After this, it goes back to a quasiperiodic attractor and then emerges a chaotic behavior with a small Lyapunov exponent. The sequence corroborates with the Lyapunov exponent profile in Figs. 2 and 4.

We emphasize that if we consider another initial condition, the results shown could be different. As we show in Sec. V, this map has multistability in the phase space, and different initial conditions can generate solutions that go to different attractors.

Our next step for the analysis of the solution in the phase space is the period of the periodic attractors, which are represented by the blue points in Fig. 6 (negative Lyapunov exponent). For this analysis, we select only the points  $(a, b)$  with a negative Lyapunov exponent and then we calculate the period of the orbit. Next, after we compute  $\lambda$  and verify if it is negative, we take the last point of the orbit as an initial condition for a time evolution of 2000 iterations in order to calculate its period. Therefore, we count the iterations that the orbit takes to return to the first point. To verify the period value, we calculate it three times and check if the three values are equivalent. If they are all equal, we plot the period value according to the color for  $(a, b)$  in the parameter space. The results for the periods of the attractors, for the same range of parameters in Fig. 6, are shown in Fig. 7.

Analyzing Fig. 7(a), we see a gray triangle shape region in the beginning of the parameter space, and this observation states that periodic attractors with period equal to 1 are more likely to exist for smaller values of  $a$ . For another small periods, such as period 2 and 3 represented by the navy blue and red points, respectively, we observe an interesting structure that appears to be periodic, and there is alternation between the red and navy blue region. In fact, this structure is similar to the Arnold tongues.<sup>2,31</sup>

In the magnification in Fig. 7(b), we see that the two lines in black, corresponding to the bifurcation diagrams in Figs. 2 and 4, intersect the period 20 (green region), and the line  $b = 0.6$  also intersects the period 40 (yellow region). If we go back to Fig. 3(b), we count a period 20 for the ghost attractor that is indicated by the red points. In Fig. 5(b), the ghost fixed points close to the chaotic band have a period equal to 40, corroborating with the result that is shown in Fig. 7(b). If we follow the line  $b = 0.6$  for values after  $a = 0.71$ , we observe the period 20, in green, followed by the period 40, in yellow, and then there is a small region of period 80 (pink region). In this way, we verify a bifurcation route of period doubling for these periodic attractors. These routes are interesting because, as is well known, the period-doubling bifurcations can also lead to a chaotic behavior in the system. In previous studies, it was stated that chaotic behavior can emerge from a period-doubling scenario in the Curry–Yorke route.<sup>21,32</sup>



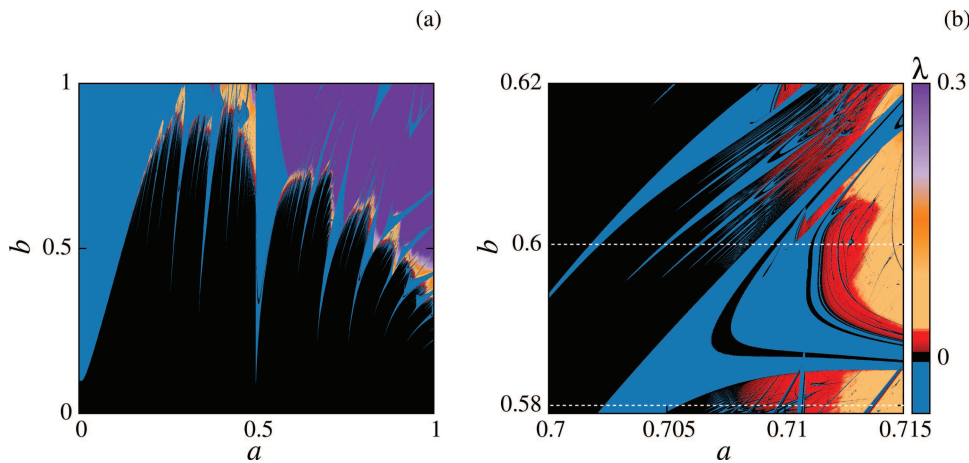


**FIG. 6.** (a) Parameter space for the Lyapunov exponent and (b) the magnification region for the bifurcation parameters shown in Figs. 2 and 4. The majority of the parameter space shows a periodic (blue points) or a quasiperiodic (black points) attractor. For high values of  $a$  and  $b$ , a chaotic behavior is possible for the system.

As we mentioned, the selection of different conditions to perform the computation of Figs. 6 and 7 can lead to a different result if we have more than one attractor in the phase space. The existence of multiple attractors is analyzed in Sec. V.

**V. MULTISTABILITY AND BASIN ENTROPY**

The multistability can be defined as the coexistence of different attractors in the phase space for one set of control parameters.<sup>33</sup> This scenario of multiattractors can be observed, for example, in situations where a weak dissipation is considered in Hamiltonian systems.<sup>34</sup> As stated in Refs. 35 and 36, the stable fixed points, in a conservative twist scenario, become periodic attractors, while the KAM curves are destroyed and the chaotic solutions are turned into transient chaos.

In order to investigate the possibility of the existence of multiple attractors in the DSNM, we study the multistability by the hysteresis of the bifurcation diagram. We fix  $b = 0.6$  and compare the two bifurcation diagrams that are obtained by increasing and

decreasing  $a$ . The diagram calculation follows the methodology used for Figs. 2 and 4. In Fig. 8(a), we plot the case where  $a$  varies from  $a = 0.0$  to  $a = 1.0$  and in Fig. 8(b), the case in which the value of  $a$  is decreased from  $a = 1.0$  to  $a = 0.0$ .

In Fig. 8, the diagram in red is significantly different when compared to the diagram in black. Up to  $a \approx 0.5$ , the diagram in red exhibits only a periodic attractor in  $y = 1.0$ , while the diagram in black shows a periodic attractor in  $y = -1.0$ , up to  $a \approx 0.2$ , and a quasiperiodic attractor up to  $a = 0.5$ . After  $a = 0.5$ , we see that periodic and quasiperiodic attractors alternate in the diagrams up to  $a \approx 0.7$  when a chaotic behavior emerges. After this point, chaotic windows alternate with quasiperiodic and periodic attractors in both diagrams. There is a window where the periodic attractors of both diagrams are symmetric in  $y$ , just before  $a = 0.75$ . For  $a > 0.75$ , the two diagrams are equivalent.

This difference between the two diagrams represents the coexistence of different attractors in the phase space. In order to illustrate this coexistence, we consider different values of  $a$  in the diagram and calculate the basins of attraction. The six chosen values for  $a$  are

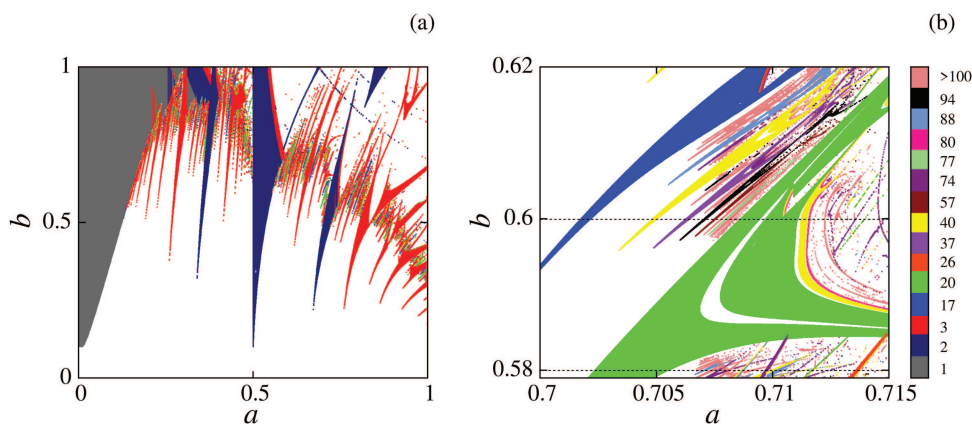


**FIG. 7.** Orbit period for the solution with a negative Lyapunov exponent ( $\lambda < 0$ ). In (a) and (b), we compute the period of the orbits for each point  $(a, b)$  with  $\lambda < 0$  in the parameter space region that are represented in Figs. 6(a) and 6(b).

06 December 2023 18:55:51

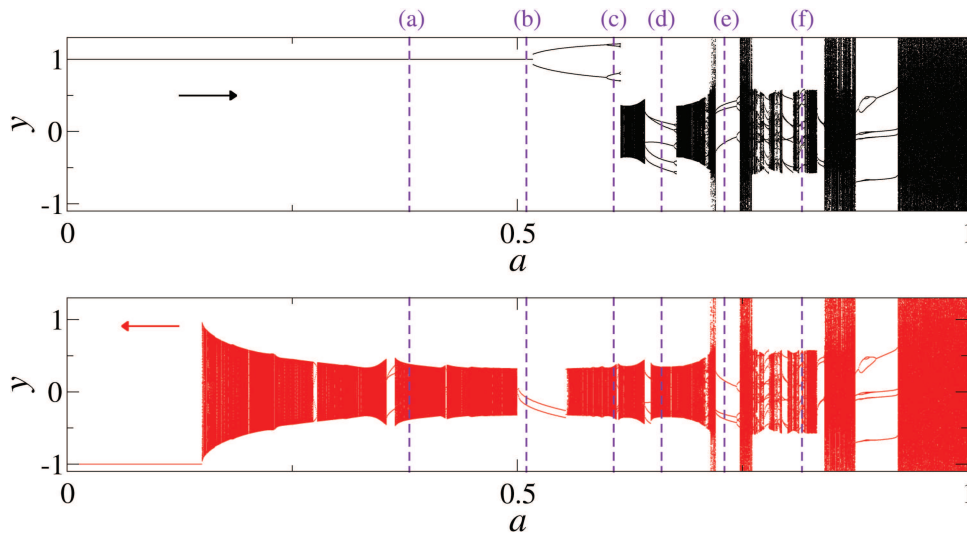


**FIG. 8.** Bifurcation diagram vs the parameter  $a$  for the DSNM with  $b = 0.6$  and  $\gamma = 0.1$ . For the black diagram, we increase the value of  $a$ , and for the red one, we start with  $a = 1.0$  and then we decrease it. We see a hysteresis between the attractors for the system. The values of  $a$  indicated by the purple dashed lines are (a)  $a = 0.380$ , (b)  $a = 0.510$ , (c)  $a = 0.607$ , (d)  $a = 0.660$ , (e)  $a = 0.730$ , and (f)  $a = 0.816$ .

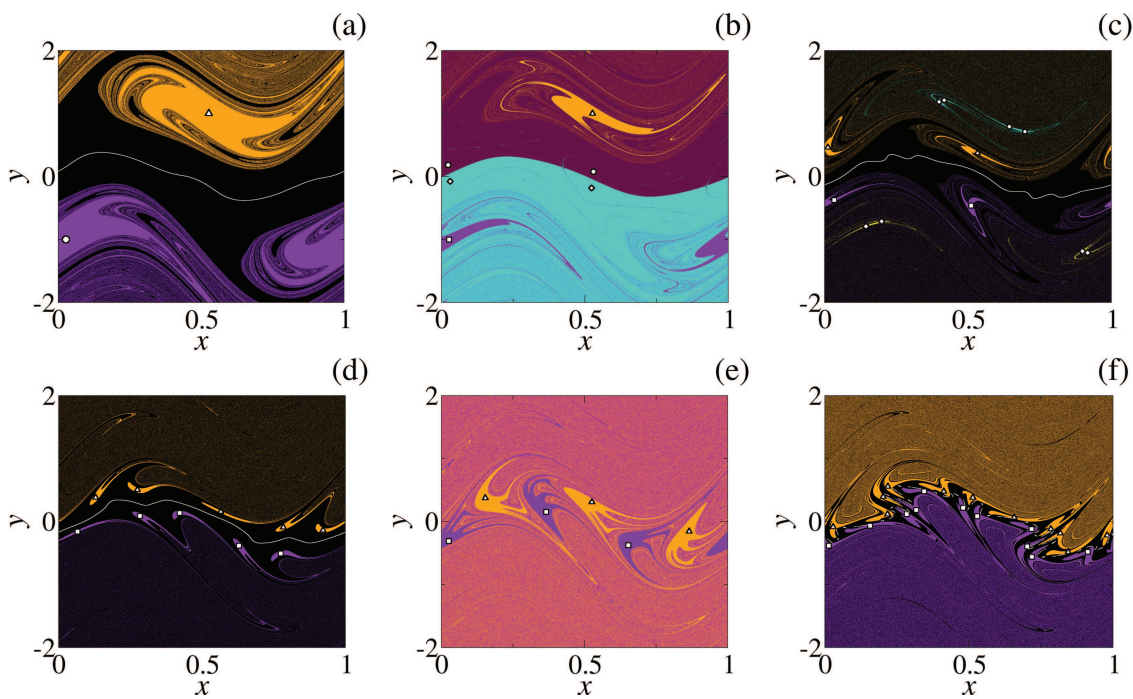


**FIG. 9.** Basins of attraction for the values of  $a$  indicated by the purple lines in Fig. 8, where each color indicates a different basin. We consider  $b = 0.6$ ,  $\gamma = 0.1$ : (a)  $a = 0.380$ , (b)  $a = 0.510$ , (c)  $a = 0.607$ , (d)  $a = 0.660$ , (e)  $a = 0.730$ , and (f)  $a = 0.816$ . The periodic attractor is indicated by geometrical symbols, while the shearless (chaotic banded) attractor is presented by a white curve (line segments).

06 December 2023 18:55:51

indicated by the violet lines in the diagrams in Fig. 8. To calculate the basin, first, we find the attractors in the phase space. After this, we construct a grid of  $3 \cdot 10^3 \times 6 \cdot 10^3$  initial conditions, linearly distributed in the phase space. Then, we iterate all the initial conditions until  $n = 10^4$  iterations and observe which attractor each orbit converges to. Each basin of attraction is assigned by a different color. The basins for the six values of  $a$  are shown in Fig. 9.

In all cases shown in Fig. 9, we see the coexistence of different attractors in the phase space. For  $a = 0.38$ ,  $a = 0.607$ , and  $a = 0.66$ , the black points represent the basin of attraction for the shearless attractor, which is indicated by the white curve in the center. The periodic attractors, in these three cases, are denoted by the geometrical symbols, and the respective basins of attractions are represented by the colored points: triangle (orange basin), square (purple basin), circle (cyan basin), and diamond (yellow basin). For  $a = 0.51$  and  $a = 0.73$ , there are only periodic attractors in the phase space. For  $a = 0.51$ , we see four different attractors: the period-one attractors that are indicated by the triangle and square with orange and purple basins, respectively, and the period-two attractors around the center that are indicated by the circle and diamond symbols with the maroon and cyan basins. For  $a = 0.73$ , there are two chains of period-three attractors, in which the triangle (square) is the attractor related to the orange (purple) basin. For  $a = 0.816$ , the result is similar to the ones presented in Figs. 9(a), 9(c), and 9(d). The black points are not related to the basin for a shearless attractor; in fact, they compose the basin of attraction for the chaotic band attractor, which is indicated by the white segments in the central region.

In Fig. 9, the basins of attraction are visually different. For  $a = 0.38$  and  $a = 0.51$ , there are regions considerably large where only one color is exhibited. The two colors are mixed in the “transition” from one color to the other. For the other cases of  $a$ , the majority of the space is composed of mixing of the basins, especially for  $a = 0.73$  where the purple and orange basins are well mixed, due to the fact that there is not a shearless attractor dividing the phase space. A mixed region represents a certain uncertainty in the final state of the solution; specifically, close initial conditions can lead to different attractors.

In order to distinguish the two cases discussed in the previous paragraph, we employ the basin entropy proposed by Daza *et al.* to quantify the uncertainty inherent to the basins.<sup>37</sup> We analyze the entropy in discretization of the phase space for a certain set of parameter values with  $N_A$  distinguishable attractors. To discretize the phase space, a finite number of boxes is placed on it. In our case, we have a bi-dimensional phase space, in which the result of the discretization is a bi-dimensional grid with  $N_T$  non-overlapping boxes. Inside each box, there is a large number of initial conditions and each one converges to one of the  $N_A$  attractors. In this way, after the construction of the basins of attraction, we have boxes with colored points inside. For each box  $i$ , we can associate an entropy, known as Gibbs entropy, defined by

$$S_i = \sum_{j=1}^{n_i} p_{i,j} \log \left( \frac{1}{p_{i,j}} \right), \tag{7}$$

where  $n_i$  is the quantity of different colors inside the box ( $n_i \in [1, N_A]$ ) and  $p_{i,j}$  is the probability of a certain color  $j$  to exist in the box  $i$ . This probability is simply computed by the division of the

**TABLE I.** Basin entropy ( $S_b$ ), boundary basin entropy ( $S_{bb}$ ), number of attractors ( $N_A$ ), and attractor types for each case of  $a$  indicated in Fig. 8. The letters P, S, and CB in the last column mean periodic, shearless, and chaotic banded, respectively.

	$S_b$	$S_{bb}$	$N_A$	Types of attractor
$a = 0.380$	0.2367	0.6106	3	P, S
$a = 0.510$	0.1532	0.3622	4	P
$a = 0.607$	0.2742	0.3813	5	P, S
$a = 0.660$	0.2783	0.3700	3	P, S
$a = 0.730$	0.5993	0.6601	2	P
$a = 0.816$	0.5519	0.6601	3	P, CB

number of points with color  $j$  by the total number of the initial conditions in the box. In this work, we consider a box with 25 initial conditions.<sup>37</sup> A non-zero value of  $S_i$  is obtained only if there is more than one color in the box.

After calculating the entropy (7) to all the  $N_T$  boxes, we compute the basin entropy  $S_b$  and the boundary basin entropy  $S_{bb}$ . These quantities are defined as<sup>37</sup>

$$S_b = \frac{S}{N_T} = \frac{1}{N_T} \sum_{i=1}^{N_T} S_i \tag{8}$$

for the basin entropy and

$$S_{bb} = \frac{S}{N_B} = \frac{1}{N_B} \sum_{i=1}^{N_T} S_i \tag{9}$$

for the boundary basin entropy, where  $N_B$  is the number of boxes in the boundary between the basins, i.e., boxes with more than one color. The basin entropy can describe the structures in the phase space<sup>38</sup> and is associated with the uncertainty of the basin, and its limit values are  $S_b = 0$  for a unique attractor and  $S_b = \log N_A$  for a completely randomized basin.<sup>37</sup> The boundary basin entropy is related to the uncertainty of the boundaries.<sup>39</sup>

For each case in Figs. 8 and 9, we calculate  $S_b$  and  $S_{bb}$  from a grid of  $2000 \times 4000$  boxes. We iterate the 25 initial conditions in each box until  $10^4$  iterations to identify the final state (the attractor). In Table I, we show the values of  $S_b$  and  $S_{bb}$ .

From the results shown in Table I, all the basins present a certain degree of uncertainty once  $S_b > 0$  for all cases. The two last cases have high values of  $S_b$ , and the region of mixed basins is larger. The lowest value for the basin entropy is in the case for  $a = 0.510$ , where the mixing is low; in fact, there is a mixing only between the orange and maroon basin and the cyan and purple ones. For the last three cases, we verify the coexistence of a shearless attractor with periodic attractors and find  $0.2 < S_b < 0.3$ . The difference between these three cases is the boundary basin entropy, which is higher for  $a = 0.380$  and almost the same for  $a = 0.607$  and  $a = 0.660$ .

Analyzing the results for the boundary basin entropy, we can divide the six cases in two situations:  $S_{bb} \approx 0.36$  and  $0.6 < S_{bb} < 0.7$ . The first situation comprises the basins for  $a = 0.510$ ,  $a = 0.607$ , and  $a = 0.660$ . We see that in the center of the basin, there is a solid region with one color around  $y = 0$  and a mixing between the basins appears for higher values of  $y$ . In the second situation, we have the

basins for  $a = 0.380$ ,  $a = 0.730$ , and  $a = 0.816$ . We verify a solid central region for  $a = 0.380$  and  $a = 0.816$ , while for  $a = 0.730$ , the solid region is around the periodic attractors. The mixing between the regions occupies the majority of the phase space for  $a = 0.730$  and  $a = 0.816$ , while for  $a = 0.380$ , the mixing is restricted to the surroundings of the fixed point attractors.

The results for the first situation are due to the solid region around  $y = 0$ . This region decreases the final value of  $S$  and also is a consequence of the large mixing region, which increases the number of  $N_B$  and decreases the value of  $S_{bb}$ . In the second situation for  $a = 0.730$  and  $a = 0.816$ , the results of  $S_b$  and  $S_{bb}$  are similar. This happens because the majority of the phase space is formed by a mixing region, and then the entropy is larger and the  $S_{bb}$  will be higher, comparing to the other cases, even if  $N_B$  is larger too. For  $a = 0.380$ , we see a smaller  $S_b$  and a larger  $S_{bb}$  as a consequence of the large solid central region, which decreases  $S$  and  $S_b$ , and the relatively small area of mixing, resulting in a small number  $N_B$  and a larger value of  $S_{bb}$ .

At last, analyzing the results for  $a = 0.380$ ,  $a = 0.660$ , and  $a = 0.816$  (all of them exhibit three distinct attractors), we see that the phase spaces with the same number of distinct attractors can present different scenarios of interaction between the basins of attraction. These different interactions are identified by different values for the basin entropy and the boundary basin entropy.

## VI. CONCLUSIONS

By the bifurcation diagrams and the construction of phase spaces, we observe two transitions in a dissipative nontwist system that were observed by Letellier *et al.*<sup>20</sup> in van der Pol oscillators. We observe the hard transition in which a quasiperiodic attractor on a torus becomes wrinkled and then chaotic, as the parameter value  $a$  varies. Changing the value of  $b$  from  $b = 0.58$  to  $b = 0.6$ , we verify the soft transition, known as the Curry–Yorke route, for the same range of  $a$ . In the Curry–Yorke route, the quasiperiodic attractor on torus breaks up in chaotic bands and then becomes a chaotic attractor.

Analyzing the parameter spaces for the Lyapunov exponent of the attractors, we see that the quasiperiodic shearless attractors show a structure similar to the parameter space for the existence of the shearless curve in the conservative map. For low values of  $a$ , the orbits exhibit a tendency to go to periodic attractors, and, as the value of  $a$  increases, the possibility of a chaotic behavior increases as well. We calculate the period of the periodic attractors, and we observe in the parameter space a structure similar to the Arnold tongues, in which the periods exhibit a certain order and a certain hierarchy.

The hysteresis in the bifurcation diagram indicates the possibility of multistability in the system. The construction of the basins of attraction shows the coexistence of three distinct attractors in the phase space: the shearless and two twin periodic attractors. The twin attractors satisfy the symmetry transformation  $T(x, y) = (x \pm 1/2, -y)$  well known for the conservative case.

We analyze the basin entropy and the boundary basin entropy in a discretization of the phase space for a set of parameter values. By means of the entropy, we find that the basins exhibit a degree of uncertainty. In our simulations, we observe that the phase

spaces with the same number of distinct attractors can show different scenarios of interaction between the basins of attraction. These different interactions can be identified through the basin entropy and the boundary basin entropy.

## ACKNOWLEDGMENTS

We wish to acknowledge the support from the Araucária Foundation, National Council for Scientific and Technological Development (CNPq), Coordination for the Improvement of Higher Education Personnel (CAPES), and São Paulo Research Foundation (FAPESP) under Grant Nos. 2018/03211–6 and 2019/07329–4. The authors would like to thank 105 Group Science ([www.105groupscience.com](http://www.105groupscience.com)) for the fruitful discussions.

## DATA AVAILABILITY

The data that support the findings of this study are available from the corresponding author upon reasonable request.

## REFERENCES

- <sup>1</sup>G. M. Zaslavsky, *Hamiltonian Chaos and Fractional Dynamics* (Oxford University Press on Demand, 2005).
- <sup>2</sup>A. J. Lichtenberg and M. A. Leiberman, *Regular and Chaotic Dynamics* (Springer, 1992), Vol. 38.
- <sup>3</sup>A. M. O. Almeida, *Hamiltonian Systems: Chaos and Quantization* (Cambridge University Press, 1990).
- <sup>4</sup>P. J. Morrison, “Magnetic field lines, Hamiltonian dynamics, and nontwist systems,” *Phys. Plasmas* **7**, 2279–2289 (2000).
- <sup>5</sup>R. S. MacKay, J. D. Meiss, and I. C. Percival, “Stochasticity and transport in Hamiltonian systems,” *Phys. Rev. Lett.* **52**, 697 (1984).
- <sup>6</sup>A. Wurm, A. Apte, and P. J. Morrison, “On reconnection phenomena in the standard nontwist map,” *Braz. J. Phys.* **34**, 1700–1706 (2004).
- <sup>7</sup>D. del Castillo-Negrete and P. J. Morrison, “Chaotic transport by Rossby waves in shear flow,” *Phys. Fluids A: Fluid Dyn.* **5**, 948–965 (1993).
- <sup>8</sup>D. del Castillo-Negrete, J. M. Greene, and P. J. Morrison, “Area preserving nontwist maps: Periodic orbits and transition to chaos,” *Physica D* **91**, 1–23 (1996).
- <sup>9</sup>J. D. Szezech, Jr., I. L. Caldas, S. R. Lopes, R. L. Viana, and P. J. Morrison, “Transport properties in nontwist area-preserving maps,” *Chaos* **19**, 043108 (2009).
- <sup>10</sup>J. D. Szezech, Jr., I. L. Caldas, S. R. Lopes, P. J. Morrison, and R. L. Viana, “Effective transport barriers in nontwist systems,” *Phys. Rev. E* **86**, 036206 (2012).
- <sup>11</sup>I. L. Caldas, R. L. Viana, C. V. Abud, J. C. D. Fonseca, Z. D. O. Guimarães Filho, T. Kroetz, F. A. Marcus, A. B. Schelin, J. D. Szezech, D. L. Toufen *et al.*, “Shearless transport barriers in magnetically confined plasmas,” *Plasma Phys. Control. Fusion* **54**, 124035 (2012).
- <sup>12</sup>M. Mugnaine, A. C. Mathias, M. S. Santos, A. M. Batista, J. D. Szezech, and R. L. Viana, “Dynamical characterization of transport barriers in nontwist Hamiltonian systems,” *Phys. Rev. E* **97**, 012214 (2018).
- <sup>13</sup>C. G. L. Martins, R. E. de Carvalho, I. L. Caldas, and M. Roberto, “Labyrinthine standard non-twist map,” *J. Phys. A: Math. Theor.* **44**, 045102 (2010).
- <sup>14</sup>R. E. De Carvalho and C. V. Abud, “Robust attractor of non-twist systems,” *Physica A* **440**, 42–48 (2015).
- <sup>15</sup>L. K. Kato and R. E. De Carvalho, “Transport barriers with shearless attractors,” *Phys. Rev. E* **99**, 032218 (2019).
- <sup>16</sup>A. Wurm and K. M. Martini, “Breakup of inverse golden mean shearless tori in the two-frequency standard nontwist map,” *Phys. Lett. A* **377**, 622–627 (2013).
- <sup>17</sup>M. Mugnaine, A. M. Batista, I. L. Caldas, J. D. Szezech, and R. L. Viana, “Ratchet current in nontwist Hamiltonian systems,” *Chaos* **30**, 093141 (2020).
- <sup>18</sup>J. P. Van der Weele and T. P. Valkering, “The birth process of periodic orbits in non-twist maps,” *Physica A* **169**, 42–72 (1990).



- <sup>19</sup>C. Simó, “Invariant curves of analytic perturbed nontwist area preserving maps,” *Regul. Chaotic Dyn.* **3**, 180–195 (1998).
- <sup>20</sup>C. Letellier, V. Messenger, and R. Gilmore, “From quasiperiodicity to toroidal chaos: Analogy between the Curry-Yorke map and the van der Pol system,” *Phys. Rev. E* **77**, 046203 (2008).
- <sup>21</sup>M. S. Baptista and I. L. Caldas, “Dynamics of the two-frequency torus breakdown in the driven double scroll circuit,” *Phys. Rev. E* **58**, 4413 (1998).
- <sup>22</sup>J. H. Curry and J. A. Yorke, “A transition from Hopf bifurcation to chaos: Computer experiments with maps on  $\mathbb{R}^2$ ,” in *The Structure of Attractors in Dynamical Systems* (Springer, 1978), pp. 48–66.
- <sup>23</sup>T. Pereira, M. S. Baptista, M. B. Reyes, I. L. Caldas, J. C. Sartorelli, and J. Kurths, “A scenario for torus T2 destruction via a global bifurcation,” *Chaos Solitons Fractals* **39**, 2198–2210 (2009).
- <sup>24</sup>T. Pereira, M. S. Baptista, M. B. Reyes, I. L. Caldas, J. C. Sartorelli, and J. Kurths, “Global bifurcation destroying the experimental torus T2,” *Phys. Rev. E* **73**, 017201 (2006).
- <sup>25</sup>J. S. E. Portela, I. L. Caldas, and R. L. Viana, “Tokamak magnetic field lines described by simple maps,” *Eur. Phys. J. Spec. Top.* **165**, 195–210 (2008).
- <sup>26</sup>S. Shinohara and Y. Aizawa, “Indicators of reconnection processes and transition to global chaos in nontwist maps,” *Prog. Theor. Phys.* **100**, 219–233 (1998).
- <sup>27</sup>J.-P. Eckmann and D. Ruelle, “Ergodic theory of chaos and strange attractors,” in *The Theory of Chaotic Attractors* (Springer, 1985), pp. 273–312.
- <sup>28</sup>M. Sandri, “Numerical calculation of Lyapunov exponents,” *Math. J.* **6**, 78–84 (1996).
- <sup>29</sup>K. Geist, U. Parlitz, and W. Lauterborn, “Comparison of different methods for computing Lyapunov exponents,” *Prog. Theor. Phys.* **83**, 875–893 (1990).
- <sup>30</sup>D. del Castillo-Negrete, J. M. Greene, and P. J. Morrison, “Renormalization and transition to chaos in area preserving nontwist maps,” *Physica D* **100**, 311–329 (1997).
- <sup>31</sup>V. I. Arnol’d, *Geometrical Methods in the Theory of Ordinary Differential Equations* (Springer, 1988).
- <sup>32</sup>R. Van Buskirk and C. Jeffries, “Observation of chaotic dynamics of coupled nonlinear oscillators,” *Phys. Rev. A* **31**, 3332 (1985).
- <sup>33</sup>A. N. Pisarchik and U. Feudel, “Control of multistability,” *Phys. Rep.* **540**, 167–218 (2014).
- <sup>34</sup>U. Feudel and C. Grebogi, “Multistability and the control of complexity,” *Chaos* **7**, 597–604 (1997).
- <sup>35</sup>M. A. Lieberman and K. Y. Tsang, “Transient chaos in dissipatively perturbed, near-integrable Hamiltonian systems,” *Phys. Rev. Lett.* **55**, 908 (1985).
- <sup>36</sup>U. Feudel, “Complex dynamics in multistable systems,” *Int. J. Bifurcat. Chaos* **18**, 1607–1626 (2008).
- <sup>37</sup>A. Daza, A. Wagemakers, B. Georgeot, D. Guéry-Odelin, and M. A. Sanjuán, “Basin entropy: A new tool to analyze uncertainty in dynamical systems,” *Sci. Rep.* **6**, 31416 (2016).
- <sup>38</sup>A. Puy, A. Daza, A. Wagemakers, and M. A. Sanjuán, “A test for fractal boundaries based on the basin entropy,” *Commun. Nonlinear Sci. Numer. Simul.* **95**, 105588 (2020).
- <sup>39</sup>A. Daza, B. Georgeot, D. Guéry-Odelin, A. Wagemakers, and M. A. Sanjuán, “Chaotic dynamics and fractal structures in experiments with cold atoms,” *Phys. Rev. A* **95**, 013629 (2017).